THE JOURNAL OF PHYSICAL CHEMISTRY LETTERS
A JOURNAL OF THE AMERICAN CHEMICAL SOCIETY

pubs.acs.org/JPCL
Letter

LHCSR1 Functions as a Dimmer Switch for Light Harvesting

Madeline P. Hoffmann,[⊥] Roberto Caferri,[⊥] Henry Lam, Stefano Capaldi, Luca Dall'Osto, Roberto Bassi,* and Gabriela S. Schlau-Cohen*

Cite This: J. Phys. Chem. Lett. 2026, 17, 7840−7851

Read Online

ACCESS | Metrics & More | Article Recommendations | Supporting Information

ABSTRACT: In oxygenic photosynthesis, high light leads to a set of photoprotective processes, known as nonphotochemical quenching, that are required for fitness. In moss and algae, the pigment−protein complex, light-harvesting stress-related (LHCSR), is crucial for photoprotection. Acidification of the thylakoid lumen under high light triggers the activation of LHCSR and the conversion of the xanthophyll violaxanthin into zeaxanthin, which is found within LHCSR. These interrelated molecular components combine to turn on a safety valve that dissipates excess energy as heat. Previous studies of detergent-solubilized LHCSR1 found that pH and zeaxanthin regulate distinct quenching sites via the protein conformation. However, protein function in the native membrane environment can be significantly different. In this work, we applied single-molecule fluorescence spectroscopy to LHCSR1 in membrane nanodiscs. The membrane environment enhanced total quenching, regardless of pH or zeaxanthin-binding. pH-dependent quenching was still observed whereas zeaxanthin-dependent quenching was suppressed. Conformational changes also increased in the membrane, establishing that the local environment can change the nature of the equilibrium between light harvesting and photoprotection.

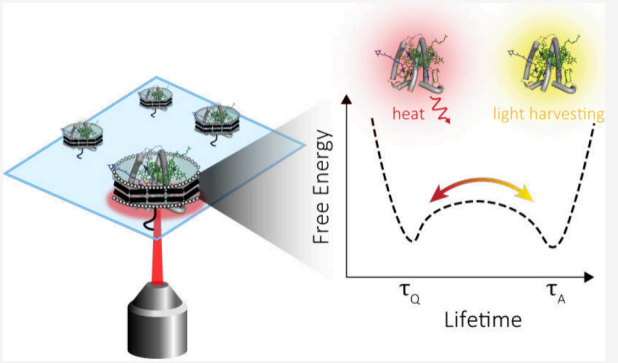

Photosynthetic reactions rely on the electron transport chain and the generation of a proton gradient across the thylakoid membrane to drive ATP and NADPH production. However, when light intensity exceeds the photosynthetic capacity, phototrophs activate photoprotective mechanisms to prevent the formation of harmful reactive oxygen species. Among these is a set of processes known as nonphotochemical quenching (NPQ), which dissipate excess energy as heat.[1,2] NPQ occurs in light-harvesting complexes (LHCs) which organize pigments within a protein scaffold. LHCs typically switch between two functions: under low light conditions, they are active, absorbing sunlight and transferring energy to the photosystems to drive charge separation and subsequent photosynthetic reactions; under high light conditions, they are quenched, dissipating the excess energy as heat via NPQ.[1,2] Conformational changes in the protein backbone of LHCs are thought to enable the switching between active and quenched states, yet the nature, number, and impact of these changes on light harvesting all remain unclear.[3−10]

The most common NPQ trigger for photosynthetic organisms is a pH drop in the thylakoid lumen. Green plants, mosses, and algae have evolved related but distinct mechanisms for sensing the lumenal acidification and switching to the quenched state.[11,12] In moss and algae, the primary trigger for pH-dependent quenching is the light-harvesting stress-related complex (LHCSR).[13−15] LHCSR expression is regulated by stress conditions, including high light,[16] nutrient deficiency,[17,18] and carbon dioxide availability.[19] Moss and algae express homologous proteins LHCSR1 and LHCSR3, where LHCSR1 overexpression is more responsive to high light.[20] Previous work has shown that LHCSR1 and LHCSR3 photoprotection is triggered in two distinct ways: pH change[21,22] and zeaxanthin binding.[23−26] Upon creation of a pH gradient, lumenal residues are protonated,[27,28] changing the structure of the protein backbone. Additionally, upon lumen acidification, the xanthophyll violaxanthin is converted to zeaxanthin via the low pH-activated enzyme violaxanthin de-epoxidase. In studies of isolated LHCSR1 in detergent, zeaxanthin binding induces quenching, even at neutral pH.[23−26] Ultrafast studies indicated a dissipative electron transfer pathway is present while dissipative energy transfer is also present in the presence of zeaxanthin at low pH.[29] These results suggest the mechanism of quenching may involve multiple photophysical processes.

Single-molecule fluorescence spectroscopy enables the observation of different photophysical states of LHCs that are averaged out in ensemble spectroscopy. By monitoring the

Received: February 15, 2026
Revised: June 1, 2026
Accepted: June 2, 2026
Published: July 6, 2026

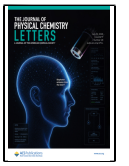

https://doi.org/10.1021/acs.jpclett.6c00541
J. Phys. Chem. Lett. 2026, 17, 7840−7851

fluorescence from individual complexes, distinct photophysical states can be identified and characterized. The LHCs are inherently dynamic due to structural changes in the protein scaffold. Chlorophyll fluorescence is highly sensitive to the surrounding protein, and so changes in these signals can be used to understand the kinetics of conformational switches and their photophysical implications.[3,30,31] State switching has been shown to be a highly sensitive reporter with differences based on the identity of the photosynthetic complex,[24,32,33] its local environment,[34−39] and its pigment composition, most notably carotenoid content.[24−26,40−42]

To date, most studies of LHCSR have either been in whole cells[13,43] or on proteins isolated in detergent.[21,44] Both approaches provide valuable insight, but also have significant drawbacks. Whole cell studies reflect the physiology of the entire organism, but interpretation of the results can be hindered by the biological complexities of intact systems. Furthermore, in whole cell studies, individual complexes cannot be isolated, precluding the use of single-molecule measurements. Studies on isolated LHCSRs allow experimental responses to be attributed directly to the protein, but may lack physiological relevance, as membrane proteins isolated in detergent can be structurally different from their native form.[45,46] Experiments on other plant LHCs, particularly light-harvesting complex II (LHCII),[37,47,48] have shown that the photophysics are modulated by the membrane environment.[34,35] Conformational changes, such as those involved in the activation of NPQ, are expected to be particularly sensitive to non-native structural perturbations. Model-membrane systems, such as nanodiscs, can be used to achieve a native-like environment while investigating isolated proteins. Nanodiscs are nanoscale discoidal lipid bilayers held together by a belting protein into which a target protein or proteins of interest can be inserted.[46]

Nanodiscs enable precise control of protein stoichiometry upon insertion,[46,49] isolating the impact of a membrane on individual LHCSR1. Proteoliposomes are another powerful model-membrane system for studying photosynthetic systems;[36,38,50] however, due to their size, they are better suited to experiments requiring multiple complexes, such as studies of the impact of aggregation,[39,51] because, with only single complexes in each proteoliposome, the protein density is an order of magnitude below native thylakoids.[52]

In this study, we used single-molecule spectroscopy to compare the conformational states and dynamics of LHCSR1 in a nanodisc to LHCSR1 in detergent with different parameters relevant to NPQ. In total, we analyzed eight sample conditions: LHCSR1 binding violaxanthin (vio LHCSR1) or zeaxanthin (zea LHCSR1), each tested at neutral pH (7.5) and low pH (4.5), in both detergent and nanodisc systems. These experiments showed that the membrane environment enhances overall quenching in LHCSR1 while suppressing the zeaxanthin-dependent effects. Together, these results reveal the local environment as an active modulator of LHCSR1 conformation, and thereby its quenching properties.

pH-Dependent LHCSR1 Quenching Being Reversible In Vitro

Vio and zea LHCSR1 proteins were purified and incorporated into nanodiscs (Figure 1A). The quality of the sample was assessed using a combination of biochemical and biophysical techniques (Supporting Information (SI) Figure S1). The absorption spectra of both vio and zea LHCSR1 remained

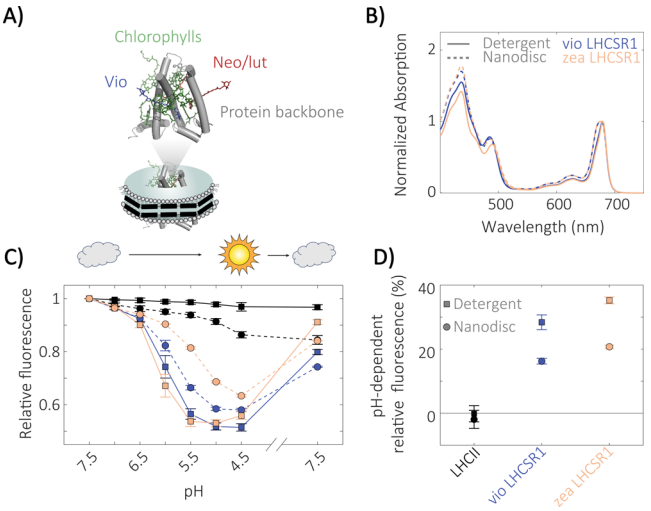

Figure 1. LHCSR1 showing pH-dependent quenching. (A) Schematic of LHCSR1 in a nanodisc consisting of a belting protein (black) and lipid bilayer (light green gradient). A detailed structural model of LHCSR1 (top) adapted from CP29 (PDB 3PL9) is shown containing chlorophylls in green, violaxanthin in purple in the L2 site, lutein in red in the L1 site, and neoxanthin in red in the N1 site. (B) Absorption spectra for LHCSR1 sample with either violaxanthin (purple) or zeaxanthin (orange), measured in detergent (solid line) or in nanodiscs (dashed line) at pH 7.5. Spectra are normalized to the Q-band. (C) Steady-state fluorescence emission intensity relative to initial intensity at pH 7.5, for LHCII (black), vio LHCSR1 (purple), and zea LHCSR1 (orange) and in detergent (solid line) and nanodiscs (dashed line) starting at pH 7.5, dropping down to pH 4.5 and then being brought back to pH 7.5. Error bars determined from three technical replicates. (D) Extent of pH-dependent quenching for LHCII (black), and LHCSR1 with violaxanthin (purple) and zea (orange) and in detergent (squares) and nanodiscs (circles) at pH 4.5 as determined from steady-state fluorescence emission experiments described in panel C.

largely unchanged in nanodiscs compared to detergent, demonstrating successful incorporation of intact protein (Figure 1B). The most notable difference in the absorbance was a slight increase in the Soret region absorbance compared to the Q-band. This signature is consistent with enhanced scattering due to the increased size of the nanodisc particles compared to detergent-solubilized protein (~13−15 nm[37,47]). A blue-shifted absorbance in the Q-band was also observed, potentially due to the configuration of LHCSR1 in the lipid environment. This is aligned with past work, which showed LHCII also exhibited a small (1 nm) blue-shift in a nanodisc environment.[47] It is likely that environmental dependent effects would be stronger in the monomeric LHCSR1 than the trimeric LHCII, as observed here.

The pH-dependent quenching of LHCSR1 in nanodiscs and detergent was evaluated using steady-state fluorescence experiments. Peak fluorescence intensity was monitored as the pH was lowered and then raised again exogenously by adding small amounts of acidic or basic solution (Figure 1C). The experiment was also performed on light-harvesting complex II (LHCII) as a control, as LHCII is not the pH sensor for triggering NPQ.

All LHCSR1 samples showed a fluorescence decrease upon pH drop (from 37% to 49%), indicating that the pH-sensing and quenching were active in vitro, including in the nanodisc. Conversely, LHCII showed a reduced fluorescence decrease upon pH drop (from 3% to 13%). These values include pH-

https://doi.org/10.1021/acs.jpclett.6c00541
J. Phys. Chem. Lett. 2026, 17, 7840−7851

Table 1. Summary of the Amplitude of Quenching Processes and Their Respective Components[a]

sample	NPQ_{max}	pH-dependent NPQ	pH-dependent NPQ (%)	nonreversible NPQ	nonreversible NPQ (%)
LHCII detergent	0.032 ± 0.017	−0.002 ± 0.011		0.033 ± 0.010	
LHCII nanodisc	0.158 ± 0.016	−0.012 ± 0.004		0.17 ± 0.012	
vio LHCSR1 detergent	0.943 ± 0.052	0.691 ± 0.061	73.18 ± 2.59	0.252 ± 0.014	26.82 ± 2.59
vio LHCSR1 nanodisc	0.723 ± 0.018	0.377 ± 0.022	52.05 ± 1.81	0.347 ± 0.005	47.94 ± 1.80
zea LHCSR1 detergent	0.789 ± 0.032	0.572 ± 0.208	90.42 ± 4.78	0.069 ± 0.048	9.58 ± 4.78
zea LHCSR1 nanodisc	0.599 ± 0.034	0.368 ± 0.037	65.78 ± 2.71	0.190 ± 0.003	34.22 ± 2.71

[a]The NPQ_{max} was calculated using the formula $\frac{F_{maxpH7.5} - F_{pH4.5}}{F_{pH4.5}}$. pH-dependent quenching was estimated using the following formula: $\left(\frac{F_{maxpH7.5}}{F_{pH4.5}}\right) - \left(\frac{F_{maxpH7.5}}{F_{pH7.5recovery}}\right)$. Non-reversible quenching was calculated as follows: $\left(\frac{F_{maxpH7.5}}{F_{pH7.5recovery}}\right) - 1$. Data are based on the steady-state fluorescence measurement performed during transition from pH 7.5 to pH 4.5 and back to pH 7.5.

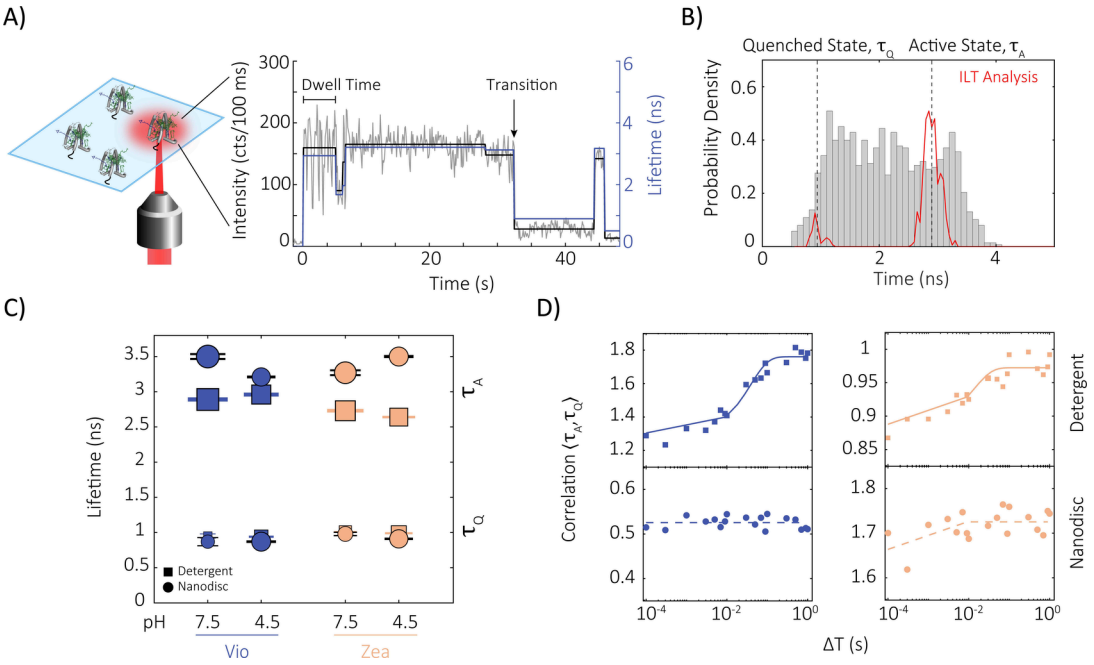

Figure 2. States and dynamics of LHCSR1. (A) Representative single-molecule trace of vio LHCSR1 in detergent at neutral pH with fluorescence intensity (gray), average intensity for each level (black), and lifetime for each level (purple). Full trace is shown in SI Figure S3. Dwell time and a level transition are indicated. (B) Representative single-molecule lifetime histogram for vio LHCSR1 in detergent at neutral pH with 1D-ILT results (red). Lifetime components obtained from 1D-ILT analysis are shown as dashed lines. Histograms and ILT overlays for all samples are shown in SI Figure S10. (C) Results of 1D-ILT analysis for all samples obtained as shown in panel B. Error bars were determined by varying the IRF position in 1D-ILT analysis. Marker size reflects the amplitudes of the quenched and active states, with larger markers indicating higher amplitudes. (D) 2D fluorescence lifetime cross-correlation with a one-component fit for violaxanthin (purple), zeaxanthin (orange), detergent (top, squares), and nanodiscs (bottom, circles) data.

dependent quenching as well as other nonreversible components. The pH was restored to 7.5 to separate these. As shown in Figure 1C, in LHCII, fluorescence did not recover upon pH increase, indicating that the loss was due to protein damage rather than a pH-induced mechanism. In contrast, the LHCSR1 samples displayed partial recovery, although to varying degrees, suggesting that protein damage also contributed to the fluorescence decrease. The extent of pH-dependent quenching was determined by calculating the percent decrease in fluorescence intensity at pH 4.5 relative to the recovered fluorescence intensity at pH 7.5 (Figure 1D). Specifically, the total NPQ, the reversible pH-dependent quenching, and the nonreversible quenching were estimated using the formulas and values reported in Table 1.

Based on these calculations, vio LHCSR1 in nanodiscs exhibited a higher NPQ value compared to zea LHCSR1 in nanodiscs, as well as higher irreversible quenching. The same trend was observed in detergent. This result suggests that violaxanthin samples underwent higher protein damage. Conversely, zeaxanthin samples displayed a stronger pH-dependent quenching and less protein damage, in accordance with the enhanced photoprotective role of zeaxanthin. Moreover, comparison between nanodisc and detergent samples showed that micelle-embedded samples displayed stronger pH-dependent quenching and less damage than those in a lipid environment.

Observation of Active and Quenched States

Ensemble fluorescence measures the average behavior arising from a heterogeneous and transient distribution of protein conformations. In contrast, single-molecule fluorescence measures the behavior of individual proteins, which can reflect the specific conformations averaged out in the ensemble measurements. To evaluate how these conformations impact

https://doi.org/10.1021/acs.jpclett.6c00541
J. Phys. Chem. Lett. 2026, 17, 7840−7851

the photophysics, single-molecule measurements were performed on vio and zea LHCSR1 in detergent and in nanodiscs at both neutral and low pH (pH 7.5 and 4.5, respectively). For each of these eight samples, LHCSR1 was immobilized at a dilute (~pM) concentration on a coverslip where the fluorescence emission was recorded for individual complexes over a period of up to 10 min. A change point finding algorithm was applied to identify changes in fluorescence intensity, with each period of constant emission having an associated intensity and lifetime.[53,54] The lifetime for each recorded period was determined by estimating the decay time scale using a single-exponential function (SI Figure S4). This model captures the overall decay as a single component, but the complex may be converting between different lifetime states on a time scale faster than the 100 ms binning time required to identify an intensity value. Therefore, the single time scale extracted for each level typically represents a weighted average of the equilibrium between underlying lifetime states, where the equilibrium is constant for each level. Representative single-molecule fluorescence intensity-lifetime traces are shown in Figure 2A and SI Figure S3.

Fluorescence periods with high intensity and long lifetimes indicate light harvesting, or the active state of LHCSR1, whereas fluorescence levels with low intensity and short lifetimes indicate photoprotection, or the quenched state. To more closely examine the fluorescence periods and their underlying functional states, histograms were constructed from the lifetime values, as illustrated for vio LHCSR1 in detergent at pH 7.5 in Figure 2A. Lifetime values were taken from the first recorded period where the influence of photoinduced degradation, which can occur due to the high fluences required for single-molecule measurements, is minimal.[55] The intensity histograms, lifetime histograms, and intensity-lifetime correlation plots are shown for all eight samples for the first recorded periods and all recorded periods in SI Figures S6, S7, S8, and S9. Notably, both the intensity and lifetime histograms had similar medians between both the first recorded periods and all recorded periods for all samples, indicating minimal effects from photoinduced degradation during our measurement window. There is a small contribution from photoinduced degradation, which typically manifests as transitions to dimmer emission, as observed in the asymmetry of the transition density plots (SI Figure S13). In single-molecule measurements, the intensity values can be influenced by many factors including the efficiency of oxygen removal to prevent singlet oxygen-induced damage, oxygen removal for triplet quenching, dim populations below the level visible in single-molecule measurements, and day-to-day fluctuations in microscope alignment. The high excitation fluences and laser repetition rates required for single-molecule measurements can also drive photophysical pathways that may not occur under lower fluences, such as singlet−triplet quenching. For these reasons, we focus on the lifetime as a window into the microscopic behaviors of interest. For all samples, the lifetime values spanned a wide range of time scales from ~0.5 ns to ~4 ns.

To quantify the populations of active and quenched states underlying the broad lifetime distributions, we used a mathematical technique known as Inverse Laplace Transform (ILT) that generates a model-free distribution of the lifetime components. Unlike the estimation performed on each recorded period, the ILT method does not assume an underlying number of components, or terms in the exponential function. A broad distribution of lifetimes from the single-exponential fits can be indicative of a wide range of underlying time scales. Alternatively, the broad distribution can arise from rapid conversion between different lifetime components faster than the binning time, with a broad distribution of the relative rates of conversion. The 1D-ILT calculation is a quasi-ensemble analysis that distinguishes between the two scenarios by analyzing the photon stream rather than the binned data. In the case of the measurements reported here, the 1D-ILT measurement established that LHCSR1 has two photophysical states across the environments and pH values.

The single-molecule data was transformed from the time domain to the lifetime domain as illustrated in Figure 2B for vio LHCSR1 in detergent at pH 7.5.[25] Two peaks were observed in the ILT distribution at ~1 ns and ~3 ns, corresponding to the quenched and active states, respectively. Based on the sensitivity of the pigment lifetime to the surrounding protein structure as well as previous work on this and other photosynthetic complexes,[9,24,25,56] we assign the active and quenched states to light-harvesting and photoprotective conformations, respectively.

The quenched and active states were present in all eight LHCSR1 samples (SI Figure S10). The values of the lifetime components are plotted in Figure 2C. The lifetime of the quenched state was well conserved across all samples. In contrast, the lifetime of the active state ranged from 2.5 ns to 3.5 ns. The lifetime of the active state was longer for the nanodisc samples than the detergent samples, but no other clear trends were observed with carotenoid and/or pH.

While the presence of the active and quenched states was consistent for all samples, their relative populations varied significantly. The populations are reflected in the amplitudes from the ILT distribution, which were estimated by integrating under the individual peaks. The amplitudes of the quenched states and active states are represented by the area of the markers (Figure 2C), with larger markers corresponding to higher amplitudes. The amplitudes of the quenched states ranged from ~10% to ~50%. For all types of LHCSR1, the amplitude increased by 5−15% from detergent to nanodiscs. The amplitudes also increased with a pH drop by ~20% and, for most samples, with conversion from violaxanthin to zeaxanthin by 5−15%, consistent with previous work and with the role of these parameters in photoprotection.[2,25,26,57] However, similar amplitudes were observed for vio and zea LHCSR1 at low pH in nanodiscs, potentially reflecting that these samples had reached the maximum level of quenching possible at the level of individual complexes. However, this result is at odds with the ensemble fluorescence intensity data, which showed that zeaxanthin nanodiscs had a greater pH quenching percent than violaxanthin nanodiscs (Figure 1D). It is possible that the most quenched zeaxanthin discs were not single-molecule visible at low pH. Another possibility is that the pH-dependent effect on violaxanthin discs at low pH was inflated due to photodamage, which ensemble data showed occurred to a greater extent in violaxanthin discs than zeaxanthin discs. Thus, the membrane environment, low pH, and zeaxanthin all generally increase the amplitude of the quenched state. The same trends were observed in the medians of the lifetime histograms (SI Figures S8 and S9). Overall, these results suggest the presence of an equilibrium between the light-harvesting and photoprotective conformations under all conditions where these parameters shift the equilibrium to modulate the level of photoprotection.

https://doi.org/10.1021/acs.jpclett.6c00541
J. Phys. Chem. Lett. 2026, 17, 7840−7851

Switching between Active and Quenched States

The ILT analysis can be further extended to look at correlations between states, which reflect the dynamics of their interconversion. This type of analysis is known as 2D-fluorescence lifetime correlation (2D-FLC) spectroscopy and was initially introduced for ensemble studies by Ishii, Tahara, and co-workers[58,59] and was subsequently extended to single-molecule studies by some of us[25,26] and then further refined by Talele and King.[60] Because of the high photon requirements of the method,[25] the 2D-FLC analysis was performed only on the neutral pH samples as the low pH samples were too quenched to accurately determine the correlations. In the 2D-FLC analysis, two types of correlations are evaluated: autocorrelations, which report on the temporal persistence of a given lifetime region, and cross-correlations, which report on exchange between different lifetime regions.[25,26] These correlations are constructed directly from pairs of detected photons separated by defined time delays. As a result, the 2D-FLC analysis has two advantages over other analyses: first, dynamics are extracted between the two lifetime states, which are resolved in the ILT but averaged out in the recorded periods; and second, the time resolution is microseconds as opposed to milliseconds to seconds because the photon stream itself is analyzed.[25,59] In samples such as LHCSR1, where lifetime distributions are broad and overlapping due to multiple underlying behaviors, 2D-FLC provides a robust and model-free means of extracting kinetic information with high temporal resolution.

To further explore the switching between states, we examined the cross-correlations for all four samples (Figure 2D, SI Figure S12). In the detergent samples, the magnitude of the cross-correlation increased with lag time (ΔT) with a sigmoidal profile, which is the canonical signature of switching between states where the rise time scale is the inverse of the sum of the forward and backward rates.[25] The correlations were noisy so a one-component fit was chosen to prevent overinterpretation of the data. Details on this fitting procedure can be found in the Materials and Methods section. For detergent samples, the forward rate constant (quenched to active) was 17.34 s^{-1} for vio LHCSR1 and 18.11 s^{-1} for zea LHCSR1. The backward rate constants were 3.54 s^{-1} and 2.63 s^{-1} respectively.

The time scale of switching between states, as extracted from the cross-correlations, is related to the energetic landscape between the two associated conformations: a faster rate means the free energy barrier between conformations is decreased. The ratio of the forward and backward rates for vio and zea LHCSR1 can be used to extract the relative populations of the active and quenched states at 1.5 for vio LHCSR1 and 1.92 for zea LHCSR1. Both samples were active biased, meaning that the active state, or light-harvesting conformation, has a lower free energy than the quenched state, or photoprotective conformation, in agreement with the 1D-ILT results that show a larger amplitude of the active as compared to the quenched state. The greater stabilization of the active state in the zeaxanthin sample as compared to the violaxanthin sample is inconsistent with the shorter lifetime of the zeaxanthin sample. This discrepancy likely indicates that the true correlation function is a multicomponent function with multiple transition pathways between the quenched and active states. Indeed, this has been shown previously.[25]

In the nanodisc samples, the cross-correlation was flat with lag time. The flat profile indicates minimal or no switching between states on the hundreds of microseconds to milliseconds time scale (SI Figure S12). However, the nonzero magnitude of the cross-correlation indicates switching between states on time scales faster than the temporal resolution, such as microsecond time scales. These flat correlations could be the result of a very small transition barrier between the quenched and active states, such that the protein can easily and quickly switch between the two conformations.

Conformational Changes Increasing in the Membrane Environment

Slower changes of the protein conformation, which alter the equilibrium between active and quenched states identified in the ILT analysis, can appear as switches between fluorescence levels. The amount of level switching can be quantitatively assessed by comparing the dwell time, which is the duration of a given fluorescence level (Figure 2A). Histograms of the dwell times for each sample were constructed and fit to a single exponential probability distribution (Figure 3A), yielding the mean dwell times. A single exponential fit function provides a simple model to capture the overall time scale, although it is

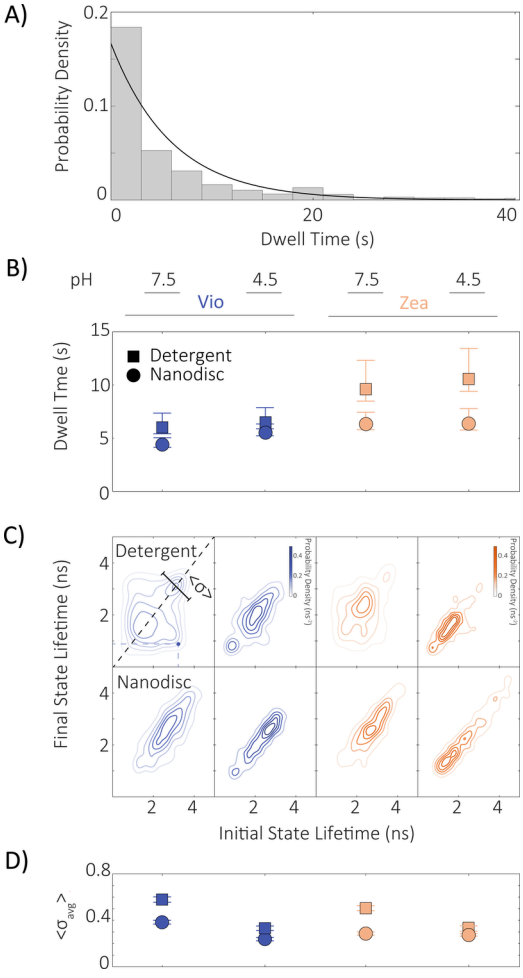

Figure 3. Transitions between fluorescence levels suppressed in nanodiscs. (A) Representative histogram of dwell times for vio LHCSR1 in detergent at pH 7.5 with exponential fit of the distribution. Histograms and fits for all samples are shown in SI Figure S11. (B) Average dwell times for all samples. Error bars were determined by bootstrapping. (C) Transition density plots for all samples. (D) Average deviation from the diagonal in the transition density plots. Error bars were determined by bootstrapping.

https://doi.org/10.1021/acs.jpclett.6c00541
J. Phys. Chem. Lett. 2026, 17, 7840−7851

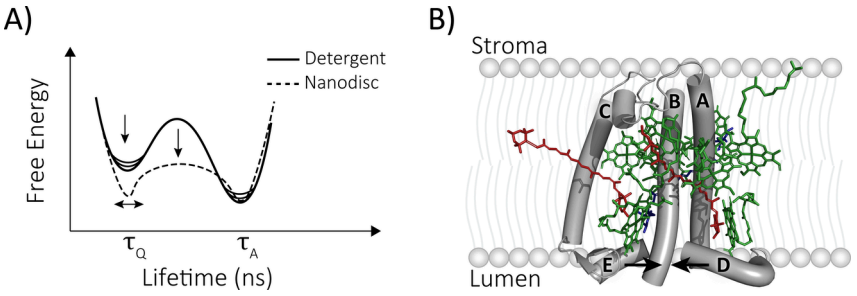

Figure 4. Model of light-harvesting and photoprotective conformations. (A) Cartoon of the free energy landscape of LHCSR1 in detergent (solid line) and nanodiscs (dashed line) that could give rise to the conformational states and transitions observed in the single-molecule data. (B) Illustration of a conformational change, such the D and E helices moving closer as indicated by the arrow, that could compact the chlorophyll and carotenoids to switch from the light-harvesting to the photoprotective conformations.

likely an oversimplification as there are long tails associated with each histogram where the fit deviates (SI Figure S11). Shorter mean dwell times reflect greater overall level switching, or increased conformational changes.

The mean dwell times for all samples are summarized in Figure 3B. LHCSR1 in a nanodisc environment exhibited shorter mean dwell times relative to their detergent counterparts, indicating that LHCSR1 is more conformationally active in a membrane environment. In detergent samples, zeaxanthin binding increased dwell times, but pH had no impact within error (Figure 3B). In contrast, in nanodisc samples, pH increased mean dwell times for vio LHCSR samples but not zea LHCSR. Similarly, zeaxanthin-binding increased dwell time for neutral pH samples, but not the low pH samples (Figure 3B).

Level switching can indicate either intrastate heterogeneity and/or interstate switching. In other words, is the protein shifting the equilibrium between the active and quenched states or changing the conformational flexibility within those states? To gain a qualitative understanding of the magnitude, and thus nature, of the switches, transition density plots were constructed. For these plots, the previous and subsequent lifetime values associated with each transition, denoted initial state and final state lifetime, were used to generate a probability density as shown in Figure 3C. On-diagonal peaks arise from small fluctuations in the lifetime values, likely reflecting changes in the conformational flexibility within a state, while off-diagonal peaks arise from large fluctuations in the values, likely reflecting significant changes to the equilibrium between states. To quantify the relative contributions of diagonal and off-diagonal peaks, the antidiagonal line width across the transition density plots was determined. The distance between each data point and the diagonal was calculated and these values were averaged to generate the line width, σ.

The σ values are plotted for all eight samples in Figure 3D. For all four conditions, the values were lower for the nanodisc samples as compared to the detergent samples. These lower values indicate that significant changes in the conformational equilibrium were actually suppressed in a membrane environment, despite the overall increase in level switching (Figure 3B). In most cases, the values were lower at pH 4.5 as compared to pH 7.5, potentially because the quenched state dominated at low pH. While the values were similar for zea LHCSR1 in nanodiscs at pH 4.5 as compared to pH 7.5, this may reflect that another factor dominates for this sample, such as the hydrophobicity of zeaxanthin.

Membrane architecture, pH, and zeaxanthin are all known to be effectors of NPQ.[2] For green algae and moss, the influence of pH and zeaxanthin on quenching in LHCSR1 has been well established.[22,23,57] Membrane architecture, however, is a complex parameter, so its role remains much more nebulous. In particular, it has been unclear whether changes to the membrane architecture impact the photophysics at the level of the individual LHCs or alter photophysical pathways through the photosystems. Such a distinction is challenging to probe in vivo. Here, we showed that the membrane environment, along with pH and zeaxanthin, set the amount of quenching in LHCSR1. Notably, the most quenched conditions could be achieved by pH and a membrane environment alone, potentially because there is a maximal level of quenching to ensure it does not impede the light-harvesting functionality of the antenna.

The single-molecule data have also revealed complex conformational dynamics; microsecond dynamics between light-harvesting and photoprotective conformations were observed from the 2D-FLC, along with transitions every few seconds that likely reflected shifts in the nature of these conformations and/or their equilibria. The membrane environment led to faster dynamics between the light-harvesting and photoprotective conformations, but the shifts in equilibria were minimal, potentially owing to the constraints associated with lateral membrane pressure (Figure 4A). These results show that LHCSR1 balances the two conformations in many different ways. Taken together, these factors may enable LHCSR1 to act as a dimmer switch, rather than an on−off switch to more flexibly respond to environmental stimuli.

To date, no experimentally obtained atomic structures of LHCSR1 or LHCSR3 are available, making it challenging to determine what membrane-mediated conformational changes are occurring. However, alignment of the amino acid sequence with Lhcb1[61] and CP29[62] has enabled computational structure predictions[10,44] that allow us to begin hypothesizing which potential quenching sites may be environmentally impacted. Following LHCII and CP29 naming conventions, LHCSR1 has three trans-membrane α-helices (A, B, and C) and two lumenal amphiphilic helices (D and E) (Figure 4B). Pigment analysis suggests that LHCSR1 binds eight chlorophylls and four carotenoids. Historically, it was thought that chlorophyll *b* only bound to LHCSRs in substoichiometric amounts,[63] but recent spectral deconvolution suggest that one or two of the chlorophyll-binding pockets may be occupied by chlorophyll *b*.[44] The identities of the carotenoid-binding pockets are likely lutein in the L1 site, violaxanthin (or zeaxanthin) in the L2 site[63,64] and lutein in the external N1 site.[63] At low pH, a

https://doi.org/10.1021/acs.jpclett.6c00541
J. Phys. Chem. Lett. 2026, 17, 7840−7851

quenching site is thought to be created in lutein in the L1 site via the rearrangement of helices C and B, triggered by the protonation in the amphiphilic helices D and/or E.[28] Zeaxanthin-mediated quenching is hypothesized to occur in the L2 binding pocket.[25] Zeaxanthin is more hydrophobic than violaxanthin which is hypothesized to lead to tighter binding in the L2 carotenoid site when the protein is in detergent. This compacts the arrangement of zeaxanthin and the neighboring chlorophylls 602 and 603, potentially creating a quenching site.[21]

Upon nanodisc incorporation, the amplitude of the quenched state increased (Figure 2C). A similar change was observed for LHCII, although to a lesser extent.[37] Cryo-EM of LHCII has shown that increased lateral pressure from a nanodisc can facilitate bringing helices D and E closer together, which allosterically regulate the transmembrane angle of helices A and B.[9] A similar effect could be at play in LHCSR1 (Figure 4B), as computational work has suggested helices D and E are important for regulating quenching sites.[28] Furthermore, such a mechanism could explain the decreased, but still present pH response in membrane nanodiscs. If the belting protein of the nanodisc already compacts the protein, then further compaction due to protonation would have less of an impact.

Interestingly, carotenoid-dependent quenching was reduced in membrane nanodiscs. These observations suggest that vio LHCSR1 has a greater conformational change upon nanodisc incorporation than zea LHCSR1, and that vio LHCSR1 adopts a structure more similar to zea LHCSR1, thus decreasing carotenoid-dependent quenching in a disc environment. The mean dwell time results also suggest that vio LHCSR1 behaves more like zea LHCSR1 in a nanodisc (Figure 3B). Water may permeate the nanodisc more than a detergent micelle,[65,66] which could lead the still hydrophobic violaxanthin to adopt a binding conformation more similar to zeaxanthin, thus increasing quenching in vio LHCSR1 to an amplitude on par with zea LHCSR1.

Overall, these results taken together clearly demonstrate that the membrane is not a neutral environment and in fact, plays a role in regulating LHCSR1 photophysics. Likely, the membrane environment modifies the conformation of the protein backbone, which in turn modifies the conformational dynamics between the active and quenched states. It appears that the membrane may enable a series of intermediate quenching levels, allowing the function of LHCSR1 to be tuned in a manner specific to the light conditions.

Plant Material and Growth Conditions

Nicotiana tabacum plants overexpressing the 6xHis-tagged LHCSR1 protein from *Physcomitrium patens* were generated as described by Pinnola et al.[67] Plants were cultivated under controlled greenhouse conditions (18−24 °C, 60% relative humidity). The presence of LHCSR1 protein was confirmed by Western blot analysis using an in-house anti-LHCSR1 antibody.

Thylakoid Isolation and Solubilization

Thylakoids were isolated following the procedure described by Morosinotto et al.[68] For protein purification, thylakoids equivalent to 500 mg of chlorophyll were solubilized with 0.5% (w/v) α-dodecyl maltoside (α-DDM, Bluepus) for 2 h at 4 °C with gentle stirring. After solubilization, insoluble material, including broken membranes and starch, was removed by centrifugation at 20000*g* for 20 min at 4 °C. The supernatant containing solubilized membrane proteins was collected for further purification.

LHCSR Protein Purification

The solubilized thylakoid membrane proteins were incubated with Ni-Sepharose resin (Chelating Sepharose Fast Flow, Cytiva) for 2 h at 4 °C under gentle stirring to purify the His-tagged LHCSR1 protein. For the zeaxanthin-binding LHCSR1 experiments, in vitro de-epoxidation was performed by treating thylakoids with 20 mM sodium ascorbate at pH 5.1 for 2 h. Following treatment, thylakoids were rapidly resuspended in 20 mM HEPES buffer (pH 7.5) and solubilized as described above.

Nanodisc Formation

Each LHCSR1 isoform was independently assembled into nanodiscs as previously reported,[47] by using a LHCSR1:MSP:lipids molar ratio of 0.125:1:120. These ratios lead to only 25% of the nanodiscs containing an LHCSR1 to ensure loading is limited to one complex. Assembled nanodiscs were further purified through a second step of IMAC and size-exclusion chromatography with a Sephadex G-200 column (Cytiva), in order to remove empty nanodiscs and aggregates, following established protocols in the field.[46] Both the quality of each assembly and the MSP:LHCSR1 stoichiometry were assessed by Coomassie-stained SDS-PAGE and negative-staining transmission electron microscopy.

Linear Absorption Spectroscopy

Absorption spectra were collected at room temperature (RT) using a SLM Aminco DW-2000 spectrophotometer in buffer containing HEPES 50 mM, NaCl 0.15 M, 20% glycerol, pH 7.5 (and 0.03% α-DM in detergent samples).

Steady-State Fluorescence Emission Spectroscopy

Fluorescence emission spectra were measured at room temperature using a Jobin−Yvon Fluoromax-3 spectrofluorometer. Samples were excited at 470 nm. Chlorophyll concentration of samples was at ∼0.02 $OD_{678\,nm}$ in 10 mM HEPES, pH 7.5, and 0.03% α-DM. Sample pH was adjusted by the incremental addition of an acidic buffer solution (0.89 M citric acid, 0.21 M disodium hydrogen phosphate) while continuously monitoring pH with a HI 2211 pH meter (HANNA Instruments) until the target value was reached. Restoration to pH 7.5 was achieved by adding 2 M NaOH, with pH monitored throughout the adjustment.

Single-Molecule Fluorescence Experiments

LHCSR1 samples were diluted to ∼40 pM in 10 mM HEPES, pH 7.5 and 0.03% α-DM (detergent samples) or 50 mM HEPES, 150 mM NaCl, pH 7.5 (nanodisc samples) and immobilized on Ni-NTA glass coverslips, giving rise to low density of complexes (SI Figure S5; Ni_{01} low-density glass coverslip, 22 mm × 22 mm; Micro- Surfaces, Englewood, NJ). His-tag immobilization was chosen for consistency between nanodisc and detergent protein samples. For the measurement at neutral pH (pH 7.5), we used an enzymatic scavenging mixture containing 2.5 mM protocatechuic acid and 25 nM protocatechuate-3,4-dioxygenase to prevent triplet oxygen formation, which has been shown to improve photophysical stability compared to other oxygen scavenger systems.[69] A mixture of 20 nM pyranose oxidase from a microorganism (Creative Enzymes, Shirley, NY), catalase (1.2 μg/mL; Sigma-Aldrich), and 100 mM glucose was used as the oxygen scavenging solution for low pH (pH 4.5) measurements, which

https://doi.org/10.1021/acs.jpclett.6c00541
J. Phys. Chem. Lett. 2026, 17, 7840−7851

has been shown to minimally alter the pH compared to other oxygen scavenger systems.[70] Single-molecule measurements were performed under a light flow of argon to further prevent oxidation damage.

Single-molecule measurements were performed on a lab-built confocal microscope described previously.[37] Excitation was performed at 610 nm by a tunable fiber laser (FemtoFiber pro, Toptica; 130 fs pulse duration, 80 MHz repetition rate). Stray light was prevented from entering the microscope using a bandpass excitation filter A630-655 nm (ET645/30x, Chroma). Excitation at 90 nW before the objective was focused using an oil immersion objective (UPLSAPO100XO, Olympus, NA 1.4). Excitation and emission were separated using a dichroic mirror (ZT647rdc, Chroma Technology) and emission was filtered using two bandpass filters (ET700/75m, Chroma and ET690/120x, Chroma) before being detected by an avalanche photodiode (SPCM-AQRH-15, Excelitas). Photon arrival times were recorded using a TCSPC module (TimeTagger20, Swabian Instruments). The IRF was measured on each day of measurements by collecting the scatter off of a coverslip without an emission filter. The IRF was 380−400 ps at full width half-maximum.

During the experiment, a 10 μm × 10 μm area of the coverslip was scanned using a 0.1 μm step size with a piezoelectric stage (Mad City Laboratories, Nano-LP100). Each 0.1 μm × 0.1 μm region was acquired at a rate of 1 scan per 0.02 s, resulting in a total acquisition time of 200 s for the full area. An excitation of approximately 30 nW before the objective was used to minimize photobleaching, which is ∼30% of the measurement power. In this scanning step, each molecule was illuminated for less than 5 s. Scanning for zeaxanthin binding LHCSR1 in detergent was done at 90 nW as molecules could not be observed at lower power. For the measurement, 90 nW excitation was then centered at the brightest spot of each molecule and fluorescence was recorded either for 10 min or until the LHCSR1 bleached. Bleaching was defined by fluorescence intensity that went below background levels (2 counts/s) and stayed there for approximately 20 seconds. The excitation level was selected based on a balance signal-to-noise and signal-to-background with photostability. Previous work on LHCII has shown this power is well below the threshold for singlet−singlet annihilation with <0.01 excitations per pulse[51,71,72] Calculations of the triplet population using the model proposed in[71] and modified in[51] adapted for the experimental conditions in this study (power, spot size, absorption cross-section) showed a population of ∼5%, indicating minimal singlet−triplet annihilation is present.

Analysis of Single-Molecule Data

Single-molecule intensity and lifetime state analysis was performed primarily as previously described.[37] Briefly, fluorescence emission was binned at 100 ms to create intensity traces. Traces were analyzed for single-molecule behavior including step changes in fluorescence behavior. Traces with exponential-like intensity decays were discarded due to likely being from aggregates. Changes in intensity were determined using the change point finding algorithm of Watkins and Yang.[53] For each intensity level determined by the intensity change point finding algorithm, the lifetime was fit with a single exponential decay using maximum likelihood estimation.[54] Single-molecule levels with intensity below background (2 counts/s) and above very high intensity (4000 counts/s) were discarded due to an inability to fit and the likelihood of the signal coming from aggregate, respectively. Additionally, levels with lifetimes below 0.5 ns were discarded due to the challenges of accurately fitting near the IRF and lifetime levels above 5 ns were discarded due to these values being unphysiological for LHCs and therefore the result of poor lifetime fitting. Single-molecule levels with less than 50 photons were discarded due to the inability to get a good lifetime fit. The subset of first levels that passed all of these criteria are referred to as "filtered first levels", while those that failed the criteria were discarded.

Dwell Time Analysis

Dwell time analysis was carried out on all single-molecule levels meeting the filtering criteria described above for the first 45 s of each trace. Traces were cut at 45 s to prevent the inclusion of photodamaged kinetics as much as possible. The dwell time distributions were fit to a single-exponential probability distribution.

1D-ILT Analysis

1D-ILT was performed to extract the number of lifetime states in a model-free manner. In short, the photons were transformed from the time domain to the lifetime domain. This was done using the maximum entropy method as described previously.[25,37,73] The amplitude $\alpha_{1,2}$ and lifetime, $\tau_{1,2}$ of each state were determined by

$$\alpha_1 = \frac{\int_{\text{peak1}} a(\tau)}{\int_{\text{all}} a(\tau)} \tag{1}$$

$$\tau_1 = \frac{\int_{\text{peak1}} \tau a(\tau)}{\int_{\text{peak1}} a(\tau)} \tag{2}$$

Error bars on the amplitude and lifetime were determined by taking the standard deviation of the five IRF shift positions closest to the minimum, as the fit was determined to be quite sensitive to the IRF position.

2D-FLC Analysis

2D fluorescence lifetime correlations were calculated as previously described,[25] however the correlation fitting procedure was slightly modified. Briefly, we performed the following analysis. The 1D-ILT distribution was first used to estimate the total number of and lifetime of quenched and active states. Next, a 2D fluorescence decay (2D-FD) matrix was constructed by plotting pairs of photons separated by ΔT values ranging from 10^{-4} to 0.3 s. The 2D-FD matrix was transformed from t-space to the 2D fluorescence lifetime correlation (2D-FLC) matrix in τ-space using a 2D-ILT by MEM fitting[58,59,74] The 2D-FLC matrix is made up of two functions: the fluorescence lifetime distribution, A, and the correlation function, G. The initial fluorescence lifetime distribution, A_0 was estimated using the values obtained in the 1D-ILT analysis. Then the correlation matrix, G_0, was estimated at all ΔT values with A_0 as a constant. A_0 and G_0 were used as initial parameters for the global fitting of the 2D-FDs at all ΔT values. A was treated as a global variable, and G was treated as a local variable at each ΔT (now $G(\Delta T)$). The resulting fit provides the correlation function, $G(\Delta T)$. The correlation function was normalized with respect to the total photon number in each state.

https://doi.org/10.1021/acs.jpclett.6c00541
J. Phys. Chem. Lett. 2026, 17, 7840−7851

To fit the correlation function in the simplest manner, let us consider a two-state system in the method of Ellson and Madge.[75] We have two species with distinct lifetimes (τ_1 and τ_2). The forward and backward rates are k_f and k_b, respectively. Assuming A and B are two conformations of the same molecule, and the molecule is immobilized (no diffusion), their time evolution is given as

$$\frac{d[A]}{dt} = -k_f[A] + k_b[B] \tag{3}$$

$$\frac{d[B]}{dt} = k_f[A] - k_b[B] \tag{4}$$

Therefore, the **M** matrix is given;

$$\mathbf{M} = \begin{bmatrix} -k_f & k_b \\ k_f & -k_b \end{bmatrix}$$

The two eigenvalues of the above **M** matrix are given as

$$\lambda = [0, -(k_f + k_b)]$$

The right eigenvectors are given as

$$\mathbf{E} = \begin{bmatrix} 1 & 1 \\ \frac{k_f}{k_b} & -1 \end{bmatrix}$$

The left eigenvectors ($\mathbf{E}^{-1}$) are obtained by solving the system of linear equations, where **I** is an identity matrix. Once the eigenvalues and eigenvectors are obtained, the correlation functions are given by

$$G_{ij}(\tau) = H_{ij} \sum_{s=1} \mathbf{E}_i^S \exp(\lambda^S \tau)(\mathbf{E}^{-1})_j^S \tag{5}$$

$$G_{ij}(\tau) = H_{ij} Z_{ij}(\tau) \tag{6}$$

where

$$H_{ij} = \frac{g^2 \epsilon_i E_j Q_i Q_j{}^2 L C_i}{\pi \omega^2} \tag{7}$$

and the factor g accounts for the quantum efficiency and gain of the detection systems. This factor also corrects for the optical filtering losses inherent in the experimental setup. ϵ_i, Q_i, and C_i are the extinction coefficient, fluorescence quantum yield, and concentration of the ith species. P is the laser power. ω is the beam diameter assuming a Gaussian intensity profile, i.e., where the intensity of the beam is reduced by $1/e^2$ relative to the maximum intensity. From eq 3, $Z_{ij}(\tau)$ values of a two-state system are given as

$$Z_{AA}(\tau) = \frac{1}{1+K}(1 + K \exp[-(k_f + k_b)\tau]) \tag{8}$$

$$Z_{BB}(\tau) = \frac{1}{1+K}(K + \exp[-(k_f + k_b)\tau]) \tag{9}$$

$$Z_{AB}(\tau) = \frac{1}{1+K}(1 - \exp[-(k_f + k_b)\tau]) \tag{10}$$

where $K = \frac{k_f}{k_b} = \frac{C_B}{C_A}$ and C_A and C_B are the number of molecules of A and B, respectively. By combining eqs 4 and 6−8, the correlation functions for a two-state system are given as

$$G_{AA}(\tau) = H_{AA} Z_{AA}(\tau) = \left(\frac{g 2\epsilon_A{}^2 Q_A{}^2 P^2 L C_A}{\pi \omega^2}\right)\frac{1}{C_A + C_B} \times (C_A + C_B \exp[-(k_f + k_b)\tau]) \tag{11}$$

$$G_{BB}(\tau) = H_{BB} Z_{BB}(\tau) = \left(\frac{g^2 \epsilon_B{}^2 Q_B{}^2 P^2 L C_B}{\pi \omega^2}\right)\frac{1}{C_A + C_B} \times (C_B + C_A \exp[-(k_f + k_b)\tau]) \tag{12}$$

$$G_{AB}(\tau) = H_{AB} Z_{AB}(\tau) = \left(\frac{g^2 \epsilon_A \epsilon_B Q_A Q_B P^2 L C_A}{\pi \omega^2}\right)\frac{C_B}{C_A + C_B} \times (1 - \exp[-(k_f + k_b)\tau]) \tag{13}$$

From the eqs 11 to 13, it is clear that by fitting the cross ($G_{AB}(\tau)$) and autocorrelation terms ($G_{AA}(\tau)$ and $G_{BB}(\tau)$) with the equation of the form $a \exp(-b\tau) + c$, one can obtain the sum of the rate constants; i.e.,

$$k_f + k_b = b \tag{14}$$

Thus, the auto- and cross-correlations were fit with $a \exp(-b\tau) + c$, where b was treated as a global variable. Fits can be found in SI Table S1.

The Arrhenius equation enables the calculation of the potential energy barrier for the forward and backward reactions.

$$k_f = A \exp\left(-\frac{E_f^*}{k_B T}\right) \tag{15}$$

$$k_b = A \exp\left(-\frac{E_b^*}{k_B T}\right) \tag{16}$$

Then energy between the states is calculated as follows.

$$\frac{k_f}{k_b} = \exp\left(-\frac{\Delta E}{k_B T}\right) \tag{17}$$

$$\Delta E = -k_B T \ln\left(\frac{k_f}{k_b}\right) \tag{18}$$

■ ASSOCIATED CONTENT

Supporting Information

The Supporting Information is available free of charge at https://pubs.acs.org/doi/10.1021/acs.jpclett.6c00541.

Additional methods, example data, and experimental details (PDF)

■ AUTHOR INFORMATION

Corresponding Authors

Roberto Bassi − *Laboratory of Photosynthesis and Bioenergy, Department of Biotechnology, University of Verona, Verona 37134, Italy; Accademia dei Lincei, Rome 00165, Italy;*

https://doi.org/10.1021/acs.jpclett.6c00541
J. Phys. Chem. Lett. 2026, 17, 7840−7851

Stazione Zoologica Anton Dohrn, Naples 80122, Italy; Email: r.bassi@univr.it

Gabriela S. Schlau-Cohen − *Department of Chemistry, Massachusetts Institute of Technology, Cambridge, Massachusetts 02139, United States*; orcid.org/0000-0001-7746-2981; Email: gssc@mit.edu

Authors

Madeline P. Hoffmann − *Department of Chemistry, Massachusetts Institute of Technology, Cambridge, Massachusetts 02139, United States*

Roberto Caferri − *Laboratory of Photosynthesis and Bioenergy, Department of Biotechnology, University of Verona, Verona 37134, Italy*

Henry Lam − *Department of Chemistry, Massachusetts Institute of Technology, Cambridge, Massachusetts 02139, United States*; orcid.org/0009-0007-5161-5370

Stefano Capaldi − *Laboratory of Photosynthesis and Bioenergy, Department of Biotechnology, University of Verona, Verona 37134, Italy*

Luca Dall'Osto − *Laboratory of Photosynthesis and Bioenergy, Department of Biotechnology, University of Verona, Verona 37134, Italy*

Complete contact information is available at: https://pubs.acs.org/10.1021/acs.jpclett.6c00541

Author Contributions

⊥M.P.H and R.C. contributed equally to this work.

Notes

The authors declare no competing financial interest.

■ ACKNOWLEDGMENTS

This work was primarily supported by the U.S. Department of Energy, Office of Science, Office of Basic Energy Sciences, Division of Chemical Sciences, Geosciences, and Biosciences under Award No. DE-SC0018097 to G.S.S.-C. The work was also supported by the Camille-Dreyfus Teacher-Scholar program. R.B. and L.D. acknowledge financial support from the European Research Council (ERC Advanced Grant 101053983-GrInSun). The authors thank Premashis Manna for assistance with developing the one-component correlation fitting analysis.

■ REFERENCES

(1) Blankenship, R. E. *Molecular mechanisms of photosynthesis*; John Wiley & Sons, 2014. DOI: 10.1002/9780470758472.

(2) Demmig-Adams, B.; Garab, G.; Adams, W., III; Govindjee *Non-photochemical Quenching and Energy Dissipation in Plants, Algae and Cyanobacteria*; Springer, 2014. DOI: 10.1007/978-94-017-9032-1.

(3) Kondo, T.; Chen, W. J.; Schlau-Cohen, G. S. Single-Molecule Fluorescence Spectroscopy of Photosynthetic Systems. *Chem. Rev.* **2017**, *117* (2), 860−898.

(4) Pinnola, A.; Bassi, R. Molecular mechanisms involved in plant photoprotection. *Biochem. Soc. Trans.* **2018**, *46* (2), 467−482.

(5) Ruban, A. V.; Wilson, S. The Mechanism of Non-Photochemical Quenching in Plants: Localization and Driving Forces. *Plant and Cell Physiology* **2021**, *62* (7), 1063−1072.

(6) Terentyev, V. V. Macromolecular conformational changes in photosystem II: interaction between structure and function. *Biophysical Reviews* **2022**, *14* (4), 871−886.

(7) Krüger, T. P.; Novoderezhkin, V. I.; Ilioaia, C.; van Grondelle, R. Fluorescence Spectral Dynamics of Single LHCII Trimers. *Biophys. J.* **2010**, *98*, 3093−3101.

(8) Krüger, T. P.; Ilioaia, C.; Johnson, M. P.; Ruban, A. V.; Papagiannakis, E.; Horton, P.; Van Grondelle, R. Controlled disorder in plant light-harvesting complex II explains its photoprotective role. *Biophys. J.* **2012**, *102* (11), 2669−2676.

(9) Ruan, M.; Li, H.; Zhang, Y.; Zhao, R.; Zhang, J.; Wang, Y.; Gao, J.; Wang, Z.; Wang, Y.; Sun, D.; Ding, W.; Weng, Y. Cryo-EM structures of LHCII in photo-active and photo-protecting states reveal allosteric regulation of light harvesting and excess energy dissipation. Nature Plants. *9:9 2023* **2023**, *9*, 1547−1557.

(10) Guarnetti Prandi, I.; Sláma, V.; Pecorilla, C.; Cupellini, L.; Mennucci, B. Structure of the stress-related LHCSR1 complex determined by an integrated computational strategy. Communications Biology. *5:1 2022* **2022**, *5* (1), 145.

(11) Ballottari, M.; Girardon, J.; Dall'Osto, L.; Bassi, R. Evolution and functional properties of Photosystem II light harvesting complexes in eukaryotes. *Biochimica et Biophysica Acta (BBA) - Bioenergetics* **2012**, *1817*, 143−157.

(12) Niyogi, K. K.; Truong, T. B. Evolution of flexible non-photochemical quenching mechanisms that regulate light harvesting in oxygenic photosynthesis. *Current Opinion in Plant Biology* **2013**, *16* (3), 307−314.

(13) Peers, G.; Truong, T. B.; Ostendorf, E.; Busch, A.; Elrad, D.; Grossman, A. R.; Hippler, M.; Niyogi, K. K. An ancient light-harvesting protein is critical for the regulation of algal photosynthesis. *Nature* **2009**, *462* (7272), 518−521.

(14) Alboresi, A.; Gerotto, C.; Giacometti, G. M.; Bassi, R.; Morosinotto, T. Physcomitrella patens mutants affected on heat dissipation clarify the evolution of photoprotection mechanisms upon land colonization. *Proc. Natl. Acad. Sci. U. S. A.* **2010**, *107* (24), 11128−11133.

(15) Pinnola, A.; Cazzaniga, S.; Alboresi, A.; Nevo, R.; Levin-Zaidman, S.; Reich, Z.; Bassi, R. Light-Harvesting Complex Stress-Related Proteins Catalyze Excess Energy Dissipation in Both Photosystems of Physcomitrella patens. *Plant Cell* **2015**, *27* (11), 3213−3227.

(16) Ledford, H. K.; Baroli, I.; Shin, J. W.; Fischer, B. B.; Eggen, R. I.; Niyogi, K. K. Comparative profiling of lipid-soluble antioxidants and transcripts reveals two phases of photo-oxidative stress in a xanthophyll-deficient mutant of Chlamydomonas reinhardtii. *Molecular Genetics and Genomics* **2004**, *272* (4), 470−479.

(17) Zhang, Z.; Shrager, J.; Jain, M.; Chang, C. W.; Vallon, O.; Grossman, A. R. Insights into the survival of Chlamydomonas reinhardtii during sulfur starvation based on microarray analysis of gene expression. *Eukaryotic Cell* **2004**, *3*, 1331−1348.

(18) Naumann, B.; Busch, A.; Allmer, J.; Ostendorf, E.; Zeller, M.; Kirchhoff, H.; Hippler, M. Comparative quantitative proteomics to investigate the remodeling of bioenergetic pathways under iron deficiency in Chlamydomonas reinhardtii. *PROTEOMICS* **2007**, *7* (21), 3964−3979.

(19) Ruiz-Sola, M. A.; Flori, S.; Yuan, Y.; Villain, G.; Sanz-Luque, E.; Redekop, P.; Tokutsu, R.; Kuken, A.; Tsichla, A.; Kepesidis, G.; et al. Light-independent regulation of algal photoprotection by CO2 availability. Nature Communications. *Nat. Commun.* **2023**, *14* (1), 1977.

(20) Maruyama, S.; Tokutsu, R.; Minagawa, J. Transcriptional Regulation of the Stress-Responsive Light Harvesting Complex Genes in Chlamydomonas Reinhardtii. *Plant and Cell Physiology* **2014**, *55* (7), 1304−1310.

(21) Bonente, G.; Ballottari, M.; Truong, T. B.; Morosinotto, T.; Ahn, T. K.; Fleming, G. R.; Niyogi, K. K.; Bassi, R. Analysis of LhcSR3, a Protein Essential for Feedback De-Excitation in the Green Alga Chlamydomonas reinhardtii. *PLOS Biology* **2011**, *9* (1), e1000577.

(22) Dinc, E.; Tian, L.; Roy, L. M.; Roth, R.; Goodenough, U.; Croce, R. LHCSR1 induces a fast and reversible pH-dependent fluorescence quenching in LHCII in Chlamydomonas reinhardtii cells. *Proc. Natl. Acad. Sci. U. S. A.* **2016**, *113* (27), 7673−7678.

(23) Pinnola, A.; Dall'Osto, L.; Gerotto, C.; Morosinotto, T.; Bassi, R.; Alboresi, A. Zeaxanthin Binds to Light-Harvesting Complex

Stress-Related Protein to Enhance Nonphotochemical Quenching in Physcomitrella patens. *Plant Cell* **2013**, *25* (9), 3519−3534.
(24) Kondo, T.; Pinnola, A.; Chen, W. J.; Dall'Osto, L.; Bassi, R.; Schlau-Cohen, G. S. Single-molecule spectroscopy of LHCSR1 protein dynamics identifies two distinct states responsible for multi-timescale photosynthetic photoprotection. Nature Chemistry. *9:8 2017* **2017**, *9* (8), 772−778.
(25) Kondo, T.; Gordon, J. B.; Pinnola, A.; Dall'Osto, L.; Bassi, R.; Schlau-Cohen, G. S. Microsecond and millisecond dynamics in the photosynthetic protein LHCSR1 observed by single-molecule correlation spectroscopy. *Proc. Natl. Acad. Sci. U. S. A.* **2019**, *116* (23), 11247−11252.
(26) Troiano, J. M; Perozeni, F.; Moya, R.; Zuliani, L.; Baek, K.; Jin, E.; Cazzaniga, S.; Ballottari, M.; Schlau-Cohen, G. S Identification of distinct pH- and zeaxanthin-dependent quenching in LHCSR3 from Chlamydomonas reinhardtii. *eLife* **2021**, *10*, e60383.
(27) Liguori, N.; Roy, L. M.; Opacic, M.; Durand, G.; Croce, R. Regulation of light harvesting in the green alga chlamydomonas reinhardtii: The c-terminus of lhcsr is the knob of a dimmer switch. *J. Am. Chem. Soc.* **2013**, *135* (49), 18339−18342.
(28) Pedraza-González, L.; Cignoni, E.; D'Ascenzi, J.; Cupellini, L.; Mennucci, B. How the pH Controls Photoprotection in the Light-Harvesting Complex of Mosses. *J. Am. Chem. Soc.* **2023**, *145*, 7482−7494.
(29) Pinnola, A.; Staleva-Musto, H.; Capaldi, S.; Ballottari, M.; Bassi, R.; Polívka, T. Electron transfer between carotenoid and chlorophyll contributes to quenching in the LHCSR1 protein from Physcomitrella patens. *Biochimica et Biophysica Acta (BBA) - Bioenergetics* **2016**, *1857*, 1870−1878.
(30) Krüger, T. P.; van Grondelle, R. Design principles of natural light-harvesting as revealed by single molecule spectroscopy. *Physica B: Condensed Matter* **2016**, *480*, 7−13.
(31) Krüger, T. P.; Wientjes, E.; Croce, R.; Van Grondelle, R. Conformational switching explains the intrinsic multifunctionality of plant light-harvesting complexes. *Proc. Natl. Acad. Sci. U.S.A.* **2011**, *108* (33), 13516−13521.
(32) Krüger, T. P.; Ilioaia, C.; Johnson, M. P.; Belgio, E.; Horton, P.; Ruban, A. V.; Van Grondelle, R. The specificity of controlled protein disorder in the photoprotection of plants. *Biophys. J.* **2013**, *105* (4), 1018−1026.
(33) Gwizdala, M.; Berera, R.; Kirilovsky, D.; van Grondelle, R.; Krüger, T. P. J. Controlling Light Harvesting with Light. *J. Am. Chem. Soc.* **2016**, *138* (36), 11616−11622.
(34) Gruber, J. M.; Scheidelaar, S.; Van Roon, H.; Dekker, J. P.; Killian, J. A.; Van Grondelle, R. Photophysics in single light-harvesting complexes II: from micelle to native nanodisks. *Proceedings SPIE 8714, Single Molecule Spectroscopy and Superresolution Imaging IX*; SPIE, 2016; 97140A. .
(35) Krüger, T. P.; Ilioaia, C.; Valkunas, L.; Van Grondelle, R. Fluorescence intermittency from the main plant light-harvesting complex: Sensitivity to the local environment. *J. Phys. Chem. B* **2011**, *115* (18), 5083−5095.
(36) Natali, A.; Gruber, J. M.; Dietzel, L.; Stuart, M. C. A.; van Grondelle, R.; Croce, R. Light-harvesting complexes (LHCs) cluster spontaneously in membrane environment leading to shortening of their excited state lifetimes. *J. Biol. Chem.* **2016**, *291*, 16730−16739.
(37) Manna, P.; Davies, T.; Hoffmann, M.; Johnson, M. P.; Schlau-Cohen, G. S. Membrane-dependent heterogeneity of LHCII characterized using single-molecule spectroscopy. *Biophys. J.* **2021**, *120* (15), 3091−3102.
(38) Tutkus, M.; Akhtar, P.; Chmeliov, J.; Görföl, F.; Trinkunas, G.; Lambrev, P. H.; Valkunas, L. Fluorescence Microscopy of Single Liposomes with Incorporated Pigment-Proteins. *Langmuir* **2018**, *34*, 14410−14418.
(39) Tutkus, M.; Chmeliov, J.; Trinkunas, G.; Akhtar, P.; Lambrev, P. H.; Valkunas, L. Aggregation-related quenching of LHCII fluorescence in liposomes revealed by single-molecule spectroscopy. *Journal of Photochemistry and Photobiology B: Biology* **2021**, *218*, 112174.
(40) Schlau-Cohen, G. S.; Yang, H.-Y.; Krüger, T. P. J.; Xu, P.; Gwizdala, M.; Van Grondelle, R.; Croce, R.; Moerner, W. E. Single-molecule identification of quenched and unquenched states of LHCII. *journal of physical chemistry letters* **2015**, *6*, 860−867.
(41) Tutkus, M.; Chmeliov, J.; Rutkauskas, D.; Ruban, A. V.; Valkunas, L. Influence of the Carotenoid Composition on the Conformational Dynamics of Photosynthetic Light-Harvesting Complexes. *J. Phys. Chem. Lett.* **2017**, *8* (23), 5898−5906.
(42) Tutkus, M.; Saccon, F.; Chmeliov, J.; Venckus, O.; Ciplys, I.; Ruban, A. V.; Valkunas, L. Single-molecule microscopy studies of LHCII enriched in Vio or Zea. *Biochimica et Biophysica Acta (BBA) - Bioenergetics* **2019**, *1860* (6), 499−507.
(43) Girolomoni, L.; Cazzaniga, S.; Pinnola, A.; Perozeni, F.; Ballottari, M.; Bassi, R. LHCSR3 is a nonphotochemical quencher of both photosystems in Chlamydomonas reinhardtii. *Proc. Natl. Acad. Sci. U. S. A.* **2019**, *116* (10), 4212−4217.
(44) Perozeni, F.; Beghini, G.; Cazzaniga, S.; Ballottari, M. Chlamydomonas reinhardtii LHCSR1 and LHCSR3 proteins involved in photoprotective non-photochemical quenching have different quenching efficiency and different carotenoid affinity. *Scientific Reports* **2020**, *10* (1), 21957.
(45) Denisov, I. G.; Sligar, S. G. Nanodiscs for structural and functional studies of membrane proteins. *Nature Structural & Molecular Biology* **2016**, *23* (6), 481−486.
(46) Denisov, I. G.; Sligar, S. G. Nanodiscs in Membrane Biochemistry and Biophysics. *Chem. Rev.* **2017**, *117* (6), 4669−4713.
(47) Son, M.; Pinnola, A.; Gordon, S. C.; Bassi, R.; Schlau-Cohen, G. S. Observation of dissipative chlorophyll-to-carotenoid energy transfer in light-harvesting complex II in membrane nanodiscs. *Nat. Commun.* **2020**, *11* (1), 1295.
(48) Sardar, S.; Caferri, R.; Camargo, F. V.; Pamos Serrano, J.; Ghezzi, A.; Capaldi, S.; Dall'osto, L.; Bassi, R.; D'Andrea, C.; Cerullo, G. Molecular mechanisms of light harvesting in the minor antenna CP29 in near-native membrane lipidic environment. *J. Chem. Phys.* **2022**, *156*, 205101.
(49) Son, M.; Moya, R.; Pinnola, A.; Bassi, R.; Schlau-Cohen, G. S. Protein-Protein Interactions Induce pH-Dependent and Zeaxanthin-Independent Photoprotection in the Plant Light-Harvesting Complex, LHCII. *J. Am. Chem. Soc.* **2021**, *143* (42), 17577−17586.
(50) Elnour, H. M.; Dietzel, L.; Ramanan, C.; Büchel, C.; van Grondelle, R.; Krüger, T. P. Energy dissipation mechanisms in the FCPb light-harvesting complex of the diatom Cyclotella meneghiniana. *Biochimica et Biophysica Acta (BBA) - Bioenergetics* **2018**, *1859* (10), 1151−1160.
(51) Manna, P.; Hoffmann, M.; Davies, T.; Richardson, K. H.; Johnson, M. P.; Schlau-Cohen, G. S. Energetic driving force for LHCII clustering in plant membranes. *Science Advances* **2023**, *9* (51), eadj0807.
(52) Kirchhoff, H.; Mukherjee, U.; Galla, H. J. Molecular Architecture of the Thylakoid Membrane: Lipid Diffusion Space for Plastoquinone. *Biochemistry* **2002**, *41* (15), 4872−4882.
(53) Watkins, L. P.; Yang, H. Detection of intensity change points in time-resolved single-molecule measurements. *J. Phys. Chem. B* **2005**, *109* (1), 617−628.
(54) Maus, M.; Cotlet, M.; Hofkens, J.; Gensch, T.; De Schryver, F. C.; Schaffer, J.; Seidel, C. A. An Experimental Comparison of the Maximum Likelihood Estimation and Nonlinear Least-Squares Fluorescence Lifetime Analysis of Single Molecules. *Anal. Chem.* **2001**, *73* (9), 2078−2086.
(55) Wang, Q.; Moerner, W. E. Dissecting pigment architecture of individual photosynthetic antenna complexes in solution. *Proc. Nat. Acad. Sci.* **2015**, *112* (45), 13880−13885.
(56) Liguori, N.; Periole, X.; Marrink, S. J.; Croce, R. From light-harvesting to photoprotection: structural basis of the dynamic switch of the major antenna complex of plants (LHCII). *Scientific Reports 2015 5:1* **2015**, *5* (1), 1−10.
(57) Bagchus, C.; Ramakers, L. A. I.; Verhoeven, D.; Beraldo, C.; Alboresi, A.; Morosinotto, T.; van Amerongen, H.; Wientjes, E. Quantitative decomposition of non-photochemical quenching in

Physcomitrium patens highlights synergistic roles of LhcSR and zeaxanthin. *Biochimica et Biophysica Acta (BBA) - Bioenergetics* **2026**, *1867*, 149581.
(58) Ishii, K.; Tahara, T. Two-dimensional fluorescence lifetime correlation spectroscopy. 2. Application. *J. Phys. Chem. B* **2013**, *117* (39), 11423−11432.
(59) Ishii, K.; Tahara, T. Two-dimensional fluorescence lifetime correlation spectroscopy. 1 Principle. *J. Phys. Chem. B* **2013**, *117* (39), 11414−11422.
(60) Talele, S.; King, J. T. Fast and robust two-dimensional inverse Laplace transformation of single-molecule fluorescence lifetime data. *Biophys. J.* **2021**, *120* (20), 4590−4599.
(61) Wan, T.; Li, M.; Zhao, X.; Zhang, J.; Liu, Z.; Chang, W. Crystal structure of a multilayer packed major light-harvesting complex: Implications for grana stacking in higher plants. *Molecular Plant* **2014**, *7* (5), 916−919.
(62) Pan, X.; Li, M.; Wan, T.; Wang, L.; Jia, C.; Hou, Z.; Zhao, X.; Zhang, J.; Chang, W. Structural insights into energy regulation of light-harvesting complex CP29 from spinach. *Nature Structural & Molecular Biology* **2011**, *18* (3), 309−315.
(63) Pinnola, A.; Ballottari, M.; Bargigia, I.; Alcocer, M.; D'Andrea, C.; Cerullo, G.; Bassi, R. Functional modulation of LHCSR1 protein from Physcomitrella patens by zeaxanthin binding and low pH. Scientific Reports. *7:1 2017* **2017**, *7* (1), 1−14.
(64) Liguori, N.; Novoderezhkin, V.; Roy, L. M.; Van Grondelle, R.; Croce, R. Excitation dynamics and structural implication of the stress-related complex LHCSR3 from the green alga Chlamydomonas reinhardtii. *Biochimica et Biophysica Acta (BBA) - Bioenergetics* **2016**, *1857* (9), 1514−1523.
(65) Maingi, V.; Rothemund, P. W. Properties of DNA-and Protein-Scaffolded Lipid Nanodiscs. *ACS Nano* **2021**, *15* (1), 751−764.
(66) Debnath, A.; Schäfer, L. V. Structure and Dynamics of Phospholipid Nanodiscs from All-Atom and Coarse-Grained Simulations. *J. Phys. Chem. B* **2015**, *119* (23), 6991−7002.
(67) Pinnola, A.; Ghin, L.; Gecchele, E.; Merlin, M.; Alboresi, A.; Avesani, L.; Pezzotti, M.; Capaldi, S.; Cazzaniga, S.; Bassi, R. Heterologous Expression of Moss Light-harvesting Complex Stress-related 1 (LHCSR1), the Chlorophyll a-Xanthophyll Pigment-protein Complex Catalyzing Non-photochemical Quenching, in Nicotiana sp. *J. Biol. Chem.* **2015**, *290* (40), 24340−24354.
(68) Morosinotto, T.; Segalla, A.; Giacometti, G. M.; Bassi, R. Purification of structurally intact grana from plants thylakoids membranes. *Journal of Bioenergetics and Biomembranes* **2010**, *42* (1), 37−45.
(69) Aitken, C. E.; Marshall, R. A.; Puglisi, J. D. An oxygen scavenging system for improvement of dye stability in single-molecule fluorescence experiments. *Biophys. J.* **2008**, *94* (5), 1826−1835.
(70) Swoboda, M.; Henig, J.; Cheng, H. M.; Brugger, D.; Haltrich, D.; Plumeré, N.; Schlierf, M. Enzymatic oxygen scavenging for photostability without ph drop in single-molecule experiments. *ACS Nano* **2012**, *6* (7), 6364−6369.
(71) Gruber, J. M.; Chmeliov, J.; Krüger, T. P. J.; Valkunas, L.; Van Grondelle, R. Singlet-triplet annihilation in single LHCII complexes. *Phys. Chem. Chem. Phys.* **2015**, *17* (30), 19844−19853.
(72) Duan, H.-G.; Stevens, A. L.; Nalbach, P.; Thorwart, M.; Prokhorenko, V. I.; Miller, R. J. D. Two-Dimensional Electronic Spectroscopy of Light-Harvesting Complex II at Ambient Temperature: A Joint Experimental and Theoretical Study. *J. Phys. Chem. B* **2015**, *119* (36), 12017−12027.
(73) Norris, A. C.; Oberg, C.; Spangler, L. C.; Scholes, G. D.; Schlau-Cohen, G. S. Discovery of Multiple Light-Harvesting States of the Photosynthetic Protein PE545. *J. Am. Chem. Soc.* **2024**, *146*, 27373−27381.
(74) Ishii, K.; Tahara, T. Extracting decay curves of the correlated fluorescence photons measured in fluorescence correlation spectroscopy. *Chem. Phys. Lett.* **2012**, *519*−*520*, 130−133.
(75) Elson, E. L.; Magde, D. Fluorescence correlation spectroscopy. I. Conceptual basis and theory. *Biopolymers* **1974**, *13* (1), 1−27.

https://doi.org/10.1021/acs.jpclett.6c00541
J. Phys. Chem. Lett. 2026, 17, 7840−7851